Research paper

Acta Neurobiol Exp 2016, 76: 212–224

ACTA NEUROBIOLOGIÆ EXPERIMENTALIS

Rat white matter injury model induced by endothelin-1 injection: technical modification and pathological evaluation

Hideaki Ono, Hideaki Imai*, Satoru Miyawaki, Hirofumi Nakatomi, and Nobuhito Saito

Department of Neurosurgery, Graduate School of Medicine, The University of Tokyo, Tokyo, Japan,
** Email: hiimai-nsu@umin.ac.jp*

White matter injury is an important cause of functional disability of the brain. We comprehensively analyzed a modified endothelin-1 (ET-1) injection-induced white matter injury model in the rat which is very valuable for investigating the underlying mechanisms of subcortical ischemic stroke. ET-1 was stereotactically injected into the internal capsule of the rat. To avoid complications with leakage of ET-1 into the lateral ventricle, the safest trajectory angle to the target was established. Rats with white matter injury were extensively evaluated for structural changes and functional sequelae, using motor function tests, magnetic resonance (MR) imaging, histopathology evolution, volume estimation of the lesion, and neuroanatomical identification of affected neurons using the retrograde tracer hydroxystilbamidine. Optimization of the trajectory of the ET-1 injection needle provided excellent survival rate. MR imaging visualized the white matter injury 2 days after surgery. Motor function deficit appeared temporarily after the operation. Histological studies confirmed damage of axons and myelin sheaths followed by inflammatory reaction and gliosis similar to lacunar infarction, with lesion volume of less than 1% of the whole brain. Hydroxystilbamidine injected into the lesion revealed wide spatial distribution of the affected neuronal population. Compared with prior ET-1 injection models, this method induced standardized amount of white matter damage and temporary motor function deficit in a reproducible and safe manner. The present model is valuable for studying the pathophysiology of not only ischemia, but a broader set of white matter damage conditions in the lissencephalic brain.

Key words: white matter injury, lacunar infarction, rat model, histopathology, retrograde tracing

INTRODUCTION

White matter injury is increasingly recognized as an extremely important and major cause of functional disability of the brain (Petty and Wettstein 1999, Kissela et al. 2009, Debette and Markus 2010, Lou and Yan 2012). White matter is the potential location of ischemic injury throughout life, particularly occurring with stroke in adults, and with vascular dementia and other conditions in the aging population. White matter injury leading to axonal disruption may cause disturbance of the motor and sensory functions, neurobehavioral syndromes, and cognitive impairment (Mortamais et al. 2013). Recently, white matter microstructural organization has been extensively investigated using diffusion tensor magnetic resonance (MR) imaging in normal or pathological populations (Jovicich et al. 2014, Maillard et al. 2014, 2015). White matter injury has also been investigated using animal models produced by internal cerebral hemorrhage in rats (Masuda et al. 2007, Ueda et al. 2014), anterior choroidal artery occlusion in rats (He et al. 1999, 2000), and chronic cerebral hypoperfusion models (Wakita et al. 1994, Hattori et al. 2015).

In one of the models, selective white matter injury is induced by injecting endothelin-1 (ET-1) into the internal capsule of the rat or mouse (Frost et al. 2006, Lecrux et al. 2008, Sozmen et al. 2009, Puentes et al. 2012). This model has broad applications for the evaluation of therapeutic interventions in various types of white matter damage, and also seems promising for experimental studies on diverse subjects such as cell transplantation for axonal regeneration (Liang et al. 2013, Xu et al. 2015) and dementia or depression models associated with diffuse and multi-system brain malfunction due to white matter damage under conditions of additional stress (Ben-Shimol et al. 2015, Kim et al. 2015, Li et al. 2015). Regrettably, this ET-1 injection model has not been adopted as widely as expected, presumably because of the uncertainty of survival rate and technical demands related to the small targets in the rat.

Received 28 January 2016, accepted 8 August 2016

Correspondence should be addressed to H. Imai
Email: hiimai-nsu@umin.ac.jp

The present study comprehensively evaluated the ET-1 injection-induced white matter injury model in the rat, focusing on the technical issues including modified trajectory (2.5 mm posterior and 4.2 mm lateral from the bregma, and 4.8 mm depth from the surface, angle 30° to the sagittal plane) and histopathological assessment over time. Assuming broad multi-system effects are caused by such lesions, the neuroanatomical regions related to the neuronal fibers passing through the internal capsule were identified using retrograde labeling.

METHODS

Animals

Nine-week-old Sprague-Dawley rats were obtained from Charles River Laboratories Japan (Yokohama, Kanagawa, Japan). A total of 71 animals were used in this study, and a breakdown of animal use is documented in the methods section and summarized in Supplementary Table I. The animals were housed under 12-hour light/dark cycle conditions with access to food and water ad libitum. Experimental procedures were conducted in accordance with the National Institutes of Health Guide for the Care and Use of Laboratory Animals (NIH Publications No. 8023, revised 1978). The formal approval for the experiments was obtained from the institutional review board (approved number P13-007), and all efforts were made to minimize the number of animals used and their suffering.

Preparation of the puncture needle and injection apparatus for stereotactic injection of ET-1

The injection apparatus is shown in Fig. 1. The Small Animal Stereotactic Instrument for the rat (David Kopf Instruments, Tujunga, CA) and a syringe injection pump (David Kopf Instruments) were utilized. Stereotactic injection was performed with a 27-gauge dental needle (Terumo Corporation, Tokyo, Japan) modified by removing the plastic connector in the middle and connecting the long segment of the needle via polyethylene tubing (PE20; Becton, Dickinson and Company, Franklin Lakes, NJ) to the short segment, which was attached to a microsyringe (10 µL; Hamilton Company, Reno, NV). The needle was fixed in the stereotactic frame arm (David Kopf Instruments). The microsyringe was controlled by an infusion pump (KD Scientific, Holliston, MA). Before the procedure, the microsyringe was carefully filled to the tip of the needle with normal saline to prevent air contamination (Fig. 1C). ET-1 solution 5 µL (200 pmol/µL; Peptide Institute, Inc., Ibaraki, Osaka, Japan) was carefully aspirated into the injection needle and adjacent tubing (Fig. 1D). ET-1 solution 1 µL was then injected at a constant flow rate (0.5 µL/min) controlled by the injection pump.

Stereotactic ET-1 injection into the internal capsule

To induce white matter injury, stereotactic ET-1 injection was performed as previously described (Frost et al. 2006, Lecrux et al. 2008, Puentes et al. 2012) with some modifications. Anesthesia was induced by inhalation of 4.0% halothane, and then maintained with 2.0% isoflurane in a mixture of 30% O_2 and 70% N_2O. Animals were placed in the stereotactic frame, and a burr hole was made with a drill for insertion of the needle into the left internal capsule (Figs 1A, 1B). Before each target approach, aspiration of ET-1 solution through the tip of the needle was confirmed as shown in Fig. 1D. Sham animals received the same amount of phosphate buffered saline delivered by the same method.

Optimization of the angle of injection

The posterior limb of the internal capsule was the target of injection (2.5 mm posterior and 4.2 mm lateral from the bregma, and 4.8 mm depth from the surface; Fig. 1E) (Paxinos and Watson 2007). To optimize the trajectory with the safest angle for injection, ET-1 solution 1 µL containing 0.5% methylene blue (Muto Pure Chemicals Co., Ltd., Tokyo, Japan) for color dye indication was injected at various angles of needle puncture (20°, 25°, and 30° to the sagittal plane, each n=7 animals) through corresponding positions of the burr hole. The relationship between the angle of the needle and the occurrence of respiratory distress was evaluated. Based on these findings, an angle of 30° was used for ET-1 injection.

Neurological and behavioral assessment

Motor function was evaluated using the ladder rung walking test, the forelimb placing test and the cylinder test, as described before (Schallert et al. 2000, Metz and Whishaw 2002) with some modifications. Depressive mood was evaluated at 4 weeks after operation using forced swimming test as described before (Porsolt et al. 1977, Tanaka et al. 2011) with some modifications. All data were collected and analyzed by observers unaware of the lesion placement data.

Ladder rung walking test

This test was developed to accurately assess motor deficits (Metz and Whishaw 2002, Lecrux et al. 2008). Briefly, the horizontal ladder rung walking test apparatus, assembled of side walls made of polymethyl methacrylate

and metal rungs (3 mm diameter), was arranged to create a passage. The ladder was 1 m long and elevated 30 cm above the ground from a neutral cage at the start point to a home cage at the end. The width of the alley was adjusted to about 1 cm wider than the animal to prevent turning around or backing. Before the date of surgery, the animals were trained to cross the ladder from the neutral cage to reach their home cage five times. During the training, the rungs were inserted regularly at 2 cm intervals. Animals (white matter injury: n=8 animals, sham operated: n=6 animals) were tested for motor function on this ladder apparatus before and after the operation. A camera (HDR-CX590; Sony Corporation, Tokyo, Japan) was positioned slightly ventral to the animal so that both side limbs and paw positions could be recorded simultaneously. Each paw placement was visualized image by image to determine the walking performance score. Scores were assessed as previously described (Metz and Whishaw 2002, Lecrux et al. 2008): 0=total miss, 1=deep slip, 2=slight slip, 3=replacement, 4=correction, 5=partial placement, and 6=correct placement. Median score was evaluated for both left and right limbs.

Forelimb placing test

This test was developed to assess sensorimotor/proprioceptive capacity (Schallert et al. 2000). Briefly, rats (n=8 animals with white matter injury) were held by their torsos allowing forelimbs to hang free. While holding the rat, the experimenter made gentle up and down movements in space prior to placement testing, which facilitated muscle relaxation and eliminated any struggling movements. Independent testing of each forelimb was induced by brushing the respective vibrissae on the edge of a table top once per trial for 10 trials. The percentage of failed affected right forelimb placement were determined at each time point and analyzed.

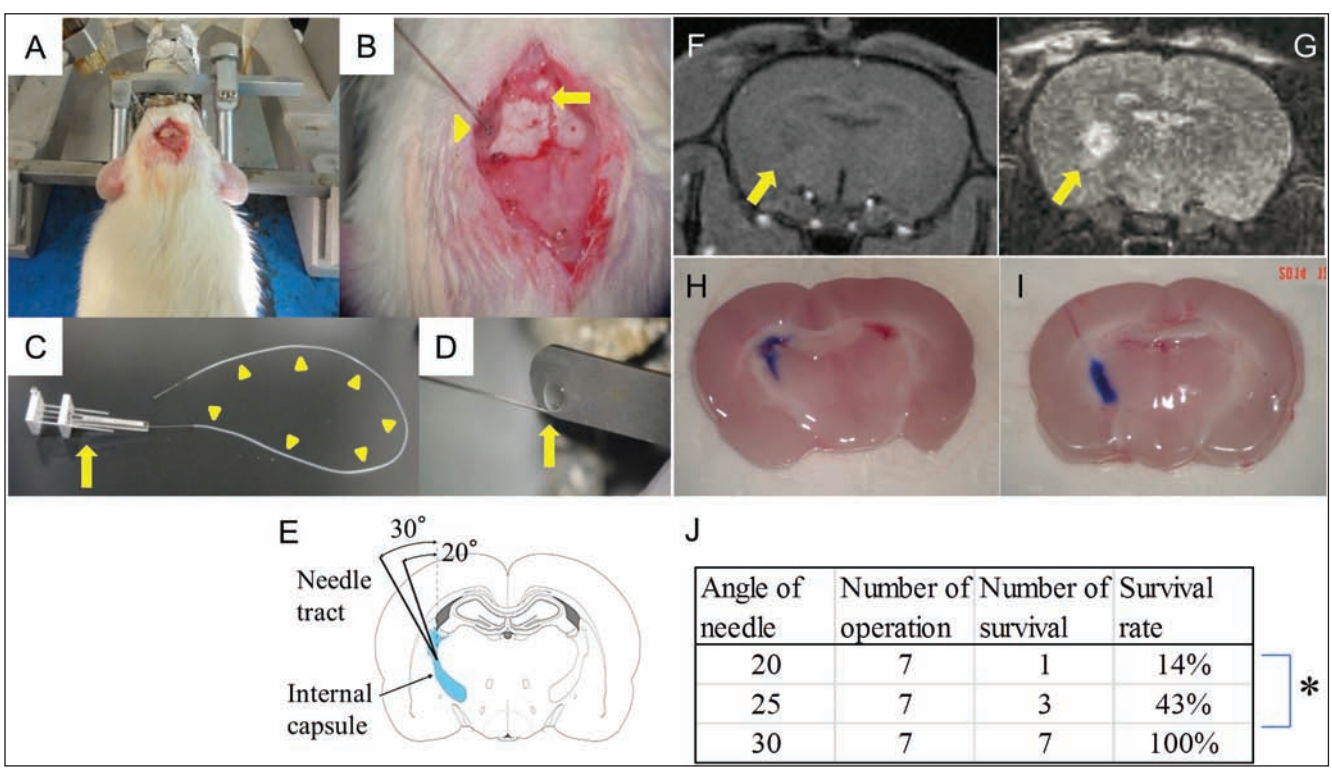

Angle of needle	Number of operation	Number of survival	Survival rate
20	7	1	14%
25	7	3	43%
30	7	7	100%

*

Fig. 1. (A–D) Photographs illustrating the procedures and equipment. (A) Rat is placed in the stereotactic frame. (B) Burr hole (arrowhead) is made, the needle is moved to the target point slowly, and endothelin-1 (ET-1) is injected (arrow: bregma). (C) Before the operation, the microsyringe (arrow), the polyethylene connecting tube (arrowheads) and the dental needle are filled carefully with normal saline to avoid air contamination. (D) Each time before puncture, ET-1 solution 5 μL (arrow) is carefully aspirated from the needle tip using the effect of surface tension. (E–J) Scheme of the target point and needle trajectories, postmortem brain sections with dye at 20° and 30°, magnetic resonance (MR) imaging findings, and relationship between angle of the needle and survival rate. (E) Target in the internal capsule (blue) was designated as 2.5 mm posterior and 4.2 mm lateral from the bregma, and 4.8 mm deep from the brain surface. Needle trajectories are shown at 20° and 30°. The tip point where the two trajectories meet is the target point. Reprinted with modification from "The Rat Brain in Stereotaxic Coordinates" (Paxinos and Watson 2007). (F, G) Typical T1 (F) and T2-weighted (G) MR image 2 days after ET-1 injection. Lesion is demonstrated on T1 weighted MR image (F, arrow) and more clearly on T2-weighted MR image as hyperintense area in the internal capsule on the operated side (G, arrow), and there are no changes on the non-operated side. (H, I) Blue dye was found in the ventricle of the rat postmortem brain using the angle of 20° (H). Blue dye was found in the internal capsule but not in the ventricle using the angle of 30° (I). (J) Relationship between the angle of the needle and survival rate after the operation. Survival rate of rats after operation increased with greater angle (*P=0.0047).

Cylinder test

This test was developed to assess the level of preference for using the unaffected forelimb for weight shifting movements during spontaneous vertical exploration (Schallert et al. 2000). Briefly, forelimb use during explorative activity was analyzed by videotaping rats (n=8 animals with white matter injury) in a transparent cylinder (20 cm diameter and 30 cm height) for 10 minutes. Mirrors were placed behind the cylinder at different angles to enable the rater to record forelimb movements when the rat was turned away from the camera. The cylindrical shape encourages vertical exploration of the walls with the forelimbs. Independent use of left or right forelimb and simultaneous use of both the left and right forelimb for contacting the wall of the cylinder were recorded. The percentage of use of the unaffected left, affected right forelimb, and both forelimbs relative to the total number of limb use were calculated, and analyzed for the difference between affected and unaffected forelimb use at each time point. If an animal was inactive, failing to rear at least once along the time course of a session, it was not included in this study.

Forced swimming test

The forced swimming test was developed to assess the depressive mood of animals, and immobile posture is thought to reflect behavioral despair. Briefly, rats (n=12 animals, 9 with white matter injury and 3 sham operated) were put in a plastic tank (25×35×60 cm) containing 30 cm of water (25±1°C) for 5 minutes. The test session was recorded using a camera, and the total duration of non-swimming, immobile time was evaluated. A rat was considered to be immobile when it remained floating in the water in an upright position, making only very small movements to keep its head above water.

Evaluation of ischemic white matter injury

MR imaging

MR imaging was performed using a dedicated small animal 1-T benchtop MR scanner (Bruker ICON 1T system [1T-MRI]; Bruker BioSpin MRI GmbH, Ettlingen, Germany). The white matter injury was evaluated at 2 days after the operation by coronal MR imaging (n=2 animals). Images were acquired using T1-weighted gradient echo and T2-weighted fast spin echo sequences with the following parameters; T1: field of view 50×50 mm, matrix 256×256, axial resolution 195 μm, repetition time 30 ms, echo time 3 ms, number of excitations 1, flip angle 25 degree, slice thickness 1 mm, total scan time 270 seconds; T2: field of view 50×50 mm, matrix 256×256, axial resolution 195 μm, repetition time 3000 ms, echo time 74 ms, number of excitations 2, flip angle 180 degree, slice thickness 0.8 mm, total scan time 312 seconds.

Histological and immunohistochemical studies

The rats were euthanized at 3 and 24 hours, and 1, 2, and 3 weeks after the ET-1 injection (n=3 animals per time point) under 4% deep halothane anesthesia and then decapitated. The brains were rapidly removed, frozen in powdered dry ice, and stored at −80°C. Coronal cryostat sections (10 μm, CM1950; Leica Microsystems, Wetzlar, Germany) along the whole extent of the lesion were placed onto glass slides and stored at −80°C until the histological and immunohistochemical analysis. Hematoxylin and eosin (HE) staining, Klüver-Barrera (KB) staining, and immunohistochemical studies using antibodies to amyloid precursor protein (APP) (MAB348; Merck Millipore, Darmstadt, Germany; diluted 1:750), glial fibrillary acidic protein (GFAP) (Z0334; Dako, Glostrup, Denmark; 1:2000), and ED1 (MCA341R; AbD Serotec, Kidlington, UK; 1:300) were performed as previously reported (Imai et al. 2006) with some modifications. Sections were observed by light microscopy (Olympus BX51; Olympus Corporation, Tokyo, Japan) and images were captured through a 20X or 40X objective lens and 10X eyepiece using a high-resolution CCD camera (Olympus DP50; Olympus Corporation).

Evaluation of white matter injury volume

To evaluate the white matter injury volume four weeks after the operation, brain sections were obtained every 200 μm throughout the whole lesion as mentioned above (n=4 animals). The sections were stained for APP and KB and examined under a microscope (BZ-X700; Keyence Corporation, Osaka, Japan). The injury area was measured by pixel counting using Photoshop CS5 software (Adobe Systems Incorporated, San Jose, CA), and the lesion volume was calculated by multiplying the injury area by the 200 μm slice thickness.

Neuroanatomical identification of cell populations associated with internal capsule injury

The neuroanatomical regions containing the axotomized neurons were identified by injection of hydroxystilbamidine (Fluoro-Gold [FG]; Fluorochrome, LLC, Denver, CO) into the internal capsule lesion (n=3 animals). To label the cortico-spinal tract after internal capsule injury, retrograde tracer FG (4%, w/v in saline, pH 7.4; Biotium, Hayward, CA) was injected 1 week after ET-1 injection. Rats were fixed on the stereotactic frame under deep anesthesia. FG 0.2 μL was injected into the internal capsule

at the same coordinates used for the injection of ET-1. Five days after FG injection, the rats were deeply anesthetized with 4% halothane and transcardially perfused with 4% paraformaldehyde in 0.1 mol/L phosphate buffer (pH 7.4). The brains were extracted and postfixed overnight, and then cut coronally. The slices were cryoprotected using graded sucrose solutions, and embedded in Tissue Tek OCT compound (Sakura Finetek USA, Torrance, CA). Coronal cryostat sections were cut at 10-μm thickness at 0.5-mm intervals throughout the brain. Sections were observed by fluorescence microscopy (Olympus BX51).

Statistical analysis

The white matter injury volume, percentage in cylinder test, and immobility time in forced swimming test are expressed as mean ±standard deviation. The walking performance scores of the ladder rung walking test and the percentage of failed affected right limb placement are shown as the median with inter-quartile range. Statistical analysis used the Student t-test for the forced swimming test, Friedman test for the walking performance score and forelimb placing test, followed by the *post hoc* Dunn test, and Wilcoxon test for the cylinder test at each time point and differences were considered significant at $P<0.05$. Fisher's exact test was used for the angle of injection and differences were considered significant at $P<0.05/3$ with Bonferroni correction.

RESULTS

Optimization of the injection angle of ET-1

Fig. 1J summarizes the success and complication rates for various angles of needle insertion for the ET-1 injection. At a needle angle of 20°, 6 of 7 rats died of respiratory depression soon after the operation. These rats did not awake from the anesthesia after operation, their breathing become shallow, and they rolled on the cage floor for about half a minute before dying about ten minutes after the injection of ET-1. Postmortem examinations in these cases confirmed high intensity of blue dye in the lateral ventricle suggesting that this needle trajectory resulted in intraventricular ET-1 leakage (Fig. 1H). At 25 degrees, only 4 of 7 rats died of respiratory depression. At 30°, all rats survived, significantly better than that at 20° ($P=0.0047$, Fig. 1J). Therefore, the angle of 30° was confirmed as safe to avoid leakage of ET-1 into the ventricle and achieve injection only into the target point (Fig. 1I). To apply this procedure with the needle at 30°, the burr hole had to be placed at the superior temporal line. As a result, the overall survival rate of the consecutive procedures was 96.4% (n=53/55 animals) in this study.

Neurological and behavioral assessment

Fig. 2 summarizes the findings of the neurological and behavioral assessments.

Ladder rung walking test

Figs 2A–2D illustrate walking performance scores for control and white matter injury animals before and after the operation. ET-1 was injected into the left internal capsule, so the right limbs were affected. Initially after the operation, rats with white matter injury showed significant decrease in walking performance score on the affected right side ($P=0.0031$), but recovered within 3 days after the operation (Fig. 2B). No significant change in score was found for the unaffected left limbs (Fig. 2A). Sham-operated rats showed no significant changes in score (Figs 2C, 2D).

Forelimb placing test

Fig. 2E shows the percentage of unsuccessful affected forelimb placing of white matter injury rats over time. Initially one day after the operation, rats with white matter injury showed significant increase in the percentage of unsuccessful affected right forelimb placings ($P=0.0048$), but recovered within three days after the operation.

Cylinder test

Fig. 2F shows the percentage of use of the unaffected left forelimb, affected right forelimb, and both forelimbs relative to the total number of limb use of white matter injury rats. Seven rats were included in this study, because one of eight rats was inactive. They showed limb use asymmetries for exploration three days after operation ($P=0.031$) with recovery after one week.

Forced swimming test

Fig. 2G shows the immobility time of rats in the forced swimming test at 4 weeks after the operation. There was no significant difference in immobility time between white matter injury rats (102.11±45.1 seconds) and sham operated rats (99.33±49.05 seconds, $P=0.929$).

Evaluation of ischemic white matter injury

MR imaging

T1- and T2-weighted MR images were obtained 2 days after ET-1 injection as shown in Figs 1F, 1G. The lesion was clearly demonstrated as a hyperintense area in the

internal capsule on the operated side and no changes on the non-operated side on T2-weighted MR imaging (Fig. 1G). The lesion could also be identified on T1-weighted imaging (Fig. 1F), but visualization was better on the T2-weighted image.

Histological and immunohistochemical findings

Fig. 3 shows the histological and immunohistochemical findings of white matter injury in chronological order. Morphological changes started 3 hours after the operation and

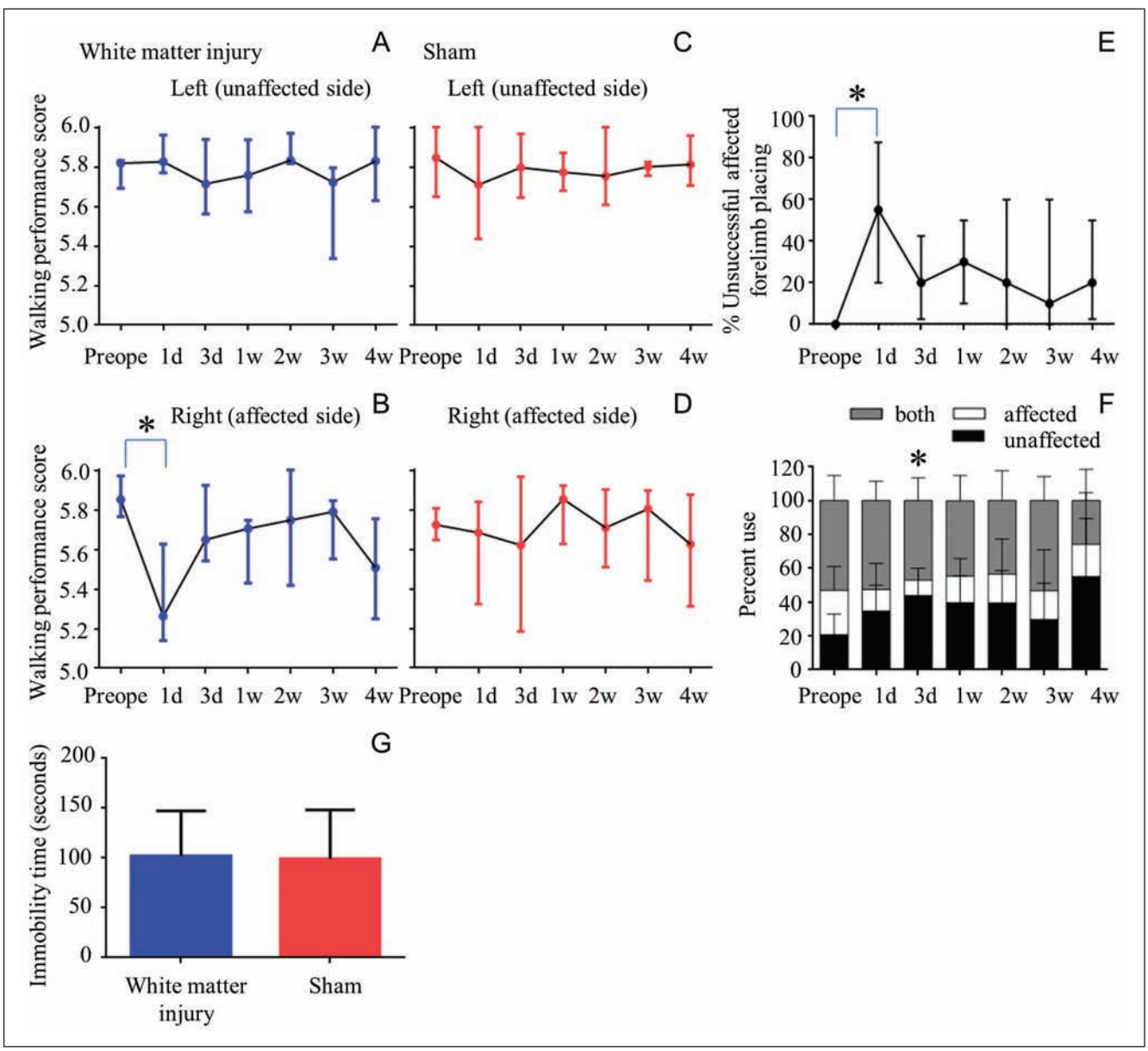

Fig. 2. Graphs illustrate the results of neurological function tests. (A–D) Walking performance scores of the ladder rung walking test are shown as the median with inter-quartile range. (A, B) Graphs showing the findings of rats with white matter injury (n=8 animals) in the unaffected left limbs (A) and affected right limbs (B). Initially after the operation, rats showed significant decrease in walking performance score in the affected right limbs (*P=0.0031), but recovered by 3 days after the operation (B). Unaffected left limbs showed no significant change in score (A). (C, D) Graphs showing the results of sham operated rats (n=6 animals) without significant changes in score. (E) The percentage of unsuccessful affected forelimb placing of white matter injury rats (n=8 animals) over time are shown as a median with inter-quartile range. One day after the operation, rats with white matter injury showed significant percentage increase of unsuccessful affected right forelimb placing (P=0.0048), but recovered within three days after the operation. (F) Percentages of use of unaffected, affected forelimb and both forelimbs relative to the total number of limb use in the cylinder test are shown as mean with standard deviation. White matter injury rats (n=7 animals) showed limb use asymmetries for exploration three days after operation (P=0.031) with recovery after one week. (G) Immobility time in the forced swimming test is shown as mean with standard deviation. There was no significant difference in immobility time between white matter injury rats (102.11±45.1 seconds) and sham operated rats (99.33±49.05 seconds, P=0.929).

were confirmed by HE staining at even lower magnification (Fig. 3A) and by specific APP immunoreactivity. Selective white matter injury, particularly axonal injury, was demonstrated by intense APP immunoreactivity in axonal swellings at the boundary of the ischemic damage area. These histological changes were followed by changes in KB staining at 24 hours after injection, indicating faint staining of damaged myelin structure, although slight changes were seen even at 3 hours after injection (Fig. 3B). To assess inflammation in the injured region over time, brain sections were immunostained with antibodies against activated microglia/macrophage antigen (ED1). Increased immunoreactivity for ED1 was observed in the lesion at 1 week after injection, but more clearly at 2 weeks, showing that activated microglia/macrophages had migrated and occupied the lesion. In addition, staining with antibodies to GFAP showed that gliosis followed the inflammatory reaction, and caused a clear boundary surrounding the lesion at more than 2 weeks after injection (Fig. 3D). No histological changes were detected on the opposite side (Fig. 3C).

Extent and volume of white matter injury

Lesions were predominantly located in the internal capsule at about 1 to 2.9 mm caudal to the bregma, as shown in Fig. 4. The volume of white matter injury was 1.83±0.29 mm^3. The lesion occupied approximately 0.16% of total brain volume.

Retrograde labeling of perikarya with FG

Fig. 5 shows the findings of FG labeling. FG was widely distributed from forebrain to brainstem. FG was detected in the cerebral cortex from rostral to caudal, and in the basal ganglia, thalamus, amygdala, brainstem, and cerebellar peduncles, as well as in the facial, vestibular, and solitary nuclei on the opposite side. On the other hand, no FG was found in the hypothalamus, hippocampus, and olfactory bulb. Details of the FG distribution are shown in Table I.

DISCUSSION

The most notable achievement in this study is the creation of a reproducible white matter injury with demonstration of robust evidence of its effects, suitable for an experimental model. At first we performed stereotactic injection of ET-1 into the internal capsule according to

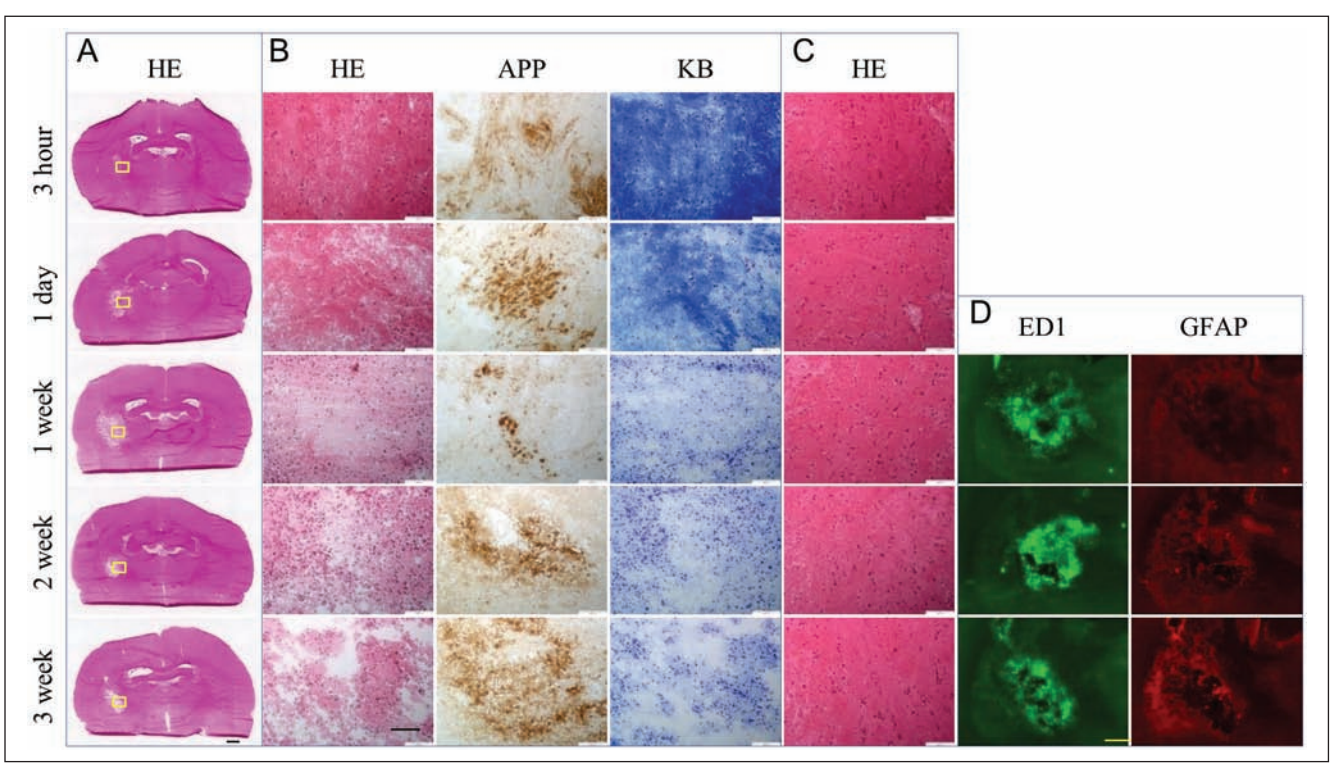

Fig. 3. Histological findings with time course. (A) White matter lesions in rat brain sections identified under lower magnification using hematoxylin and eosin (HE) staining. (B) HE and Klüver-Barrera (KB) staining and immunohistochemical staining for amyloid precursor protein (APP) of white matter injury (yellow squares in A) under higher magnification. APP-immunopositive cells were present in the lesion from 3 hours after the operation, and HE and KB staining became weaker with time. (C) No change in the internal capsule on the contralateral side on HE staining. (D) ED1-immunopositive cells accumulated in the lesion from 1 to 3 weeks, especially at 2 weeks after the operation, and glial fibrillary acidic protein (GFAP)-immunopositive cells were identified around the lesion from 2 weeks after surgery. Scale bars =1 mm (A), 100 μm (B, C), and 500 μm (D).

the original method introduced in 2006 (Frost et al. 2006), but we found respiratory distress in some animals in the process of developing our previous experimental work with this technique (Puentes et al. 2012). We assumed the possibility of ET-1 leakage into the ventricle resulting from passage of the needle, because ET-1 injected into a cerebral cistern causes respiratory distress in the rat as described in our previous experiments (Chen et al. 2013). The original procedure of stereotactic injection for internal capsule lesions was performed at an angle of 25° to the sagittal plane (Lecrux et al. 2008, Puentes et al. 2012). Our pilot study found some animals suffering from respiratory distress at that angle. Therefore, we tried to find the optimal angle for injection. Our investigation using co-injection of a blue dye with ET-1 revealed a relationship between the angle and the ventricular leakage of ET-1. We confirmed that an angle of 30° to the sagittal plane avoids passing through the lateral ventricle with high consistency (Fig. 1).

Our histological assessment indicated that this model effectively simulates lacunar infarction. Morphological damage to the white matter was detected as axonal swellings or bulges, which were immunopositive for APP at 3 hours after injection of ET-1 (Fig. 3B). KB staining revealed faint reactivity of the myelin (Fig. 3B) indicating damaged myelin sheaths at 24 hours after injection, whereas ED1 and GFAP showed no immunoreactivity. However, ED1 showed strong immunoreactivity in the lesion at 1 week after injection. GFAP immunoreactivity was also confirmed in the lesion at 2 to 3 weeks after injection. The true biochemical mechanisms of action of ET-1 on white matter are still unknown, because ET-1 targets not only endothelial and smooth muscle cells to contract small vessels and induce ischemic lesion, but also affects neurons and glia (Fuxe et al. 1992, Sasaki et al. 1997, Gilmour et al. 2004, Gadea et al. 2008). The present histological evaluation showed that the most sensitive structure in the white matter was the axon, followed by myelin. These findings are similar to our previous findings in the miniature pig lacunar infarction model (Imai et al. 2006, Tanaka et al. 2008). Furthermore, the appearance of inflammatory reaction and gliosis after the insult in this ET-1 injection model is apparently similar to that of lacunar infarction in the miniature pig induced by perforating artery occlusion. In fact, the whole sequence of morphological events detected by these studies was identical in the ET-1 and perforator occlusion models, supporting a common ischemic mechanism. In addition, the volume of white matter injury was about 1.8 mm^3, and occupied approximately 0.16% of the total brain. In humans, a lacunar infarction has diameter of about 1.5 cm and volume of about 1.77 cm^3, so this lesion occupies about 0.15% of the whole brain volume, which is about 1200 cm^3. This volumetric assessment also indicated that this model effectively simulates lacunar infarction, although it would be even better if we could also have conducted quantitative assessment of histopathology for comparison using semi-automated analysis procedures as previously reported (Wagner et al. 2013). Selective occlusion of a perforating artery to induce small infarction is impossible in small animals such as rodents. Therefore, ET-1 injection into the internal capsule of the rat appears to be the most practical method to produce selective, standardized, and reproducible white matter injury at the moment.

The present study did not identify dense motor deficits such as hemiparesis during locomotor function evaluation, suggesting that a more sensitive method for locomotor assessment in this model is required, such as the foot print test (Puentes et al. 2012). Therefore, motor function was evaluated using the ladder test, the forelimb placing test and the cylinder test as described before (Schallert et al.

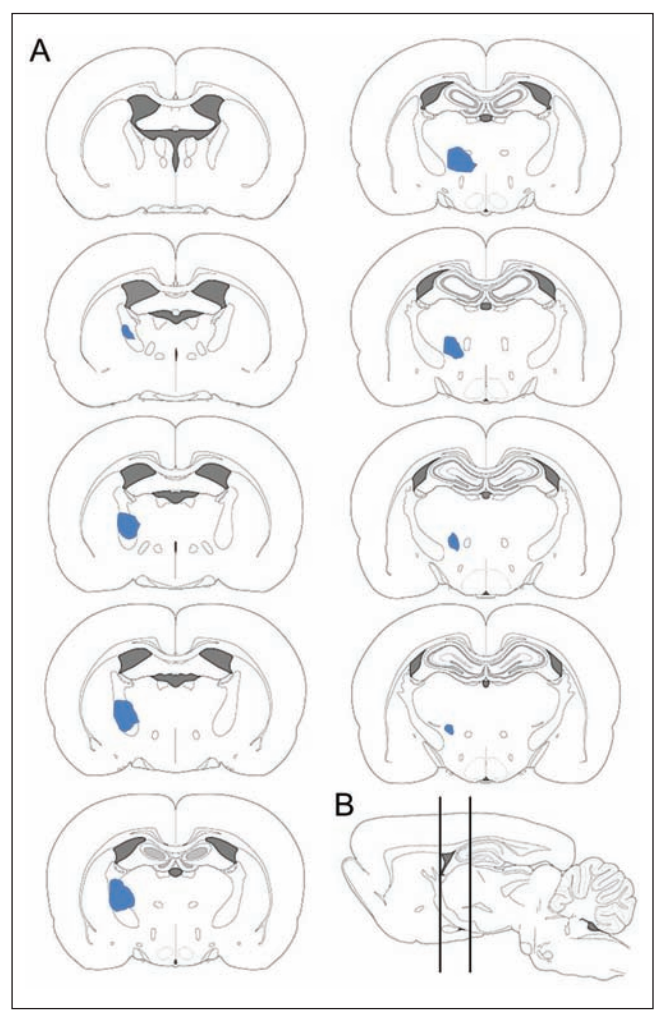

Fig. 4. Extent and volume of the white matter lesion. (A) Extent of lesions shown in blue and mapped on diagrams of brain sections modified from "The Rat Brain in Stereotaxic Coordinates" (Paxinos and Watson 2007). These coronal brain sections are 0.96 to 2.92 mm caudal from the bregma and are located between the lines of (B). Volume of white matter lesion was 1.83±0.29 mm^3.

2000, Metz and Whishaw 2002) with some modifications. Sham-operated rats showed no significant difference in walking performance score over time. In contrast, white matter injury rats showed statistically significant differences in walking performance score at 24 hours after injection (Figs 2A–2D). Also, rats with white matter injury showed significant increase in the percentage of unsuccessful affected right forelimb placings one day after operation (Fig. 2E). We found significant recovery at 3 days after injury with slower recovery of motor performance during the following days. As for the cylinder test, rats showed limb use asymmetries for exploration three days after operation with recovery after one week (Fig. 2F). The rat may have significant abilities of spontaneous recovery over time, possibly mediated by compensatory behavioral strategies to maximize the use of spared systems and mechanisms of axonal regeneration such as sprouting and remyelination (Oshima et al. 2009, Ueno et al. 2012). Although we conducted three neurological function tests in this study that apparently were not influenced by compensation or repeated testing because of their different task contents, it is still hard to discriminate accurately the true recovery from compensation (Boltze et al. 2014). To overcome this difficulty, we could have conducted other tests that could have been minimally affected by compensation or repeated testing, such as the tapered/ledged beam walking test and Montoya's staircase test, a task for our future research. In any case, this phenomenon of spontaneous recovery of locomotor function is frequently observed after lacunar infarction in patients as well as in stroke animal models (Tanaka et al. 2008, Moon et al. 2009). Moreover, the forced swimming test revealed that this model did not show apparent sign of depressive mood at 1 month after the operation. A previous study reported that WMI correlates with psychiatric disorder such as depression in humans, so WMI may be implicated in the pathogenesis of depression (Brown et al. 1992). According to the result of this study, WMI itself did not

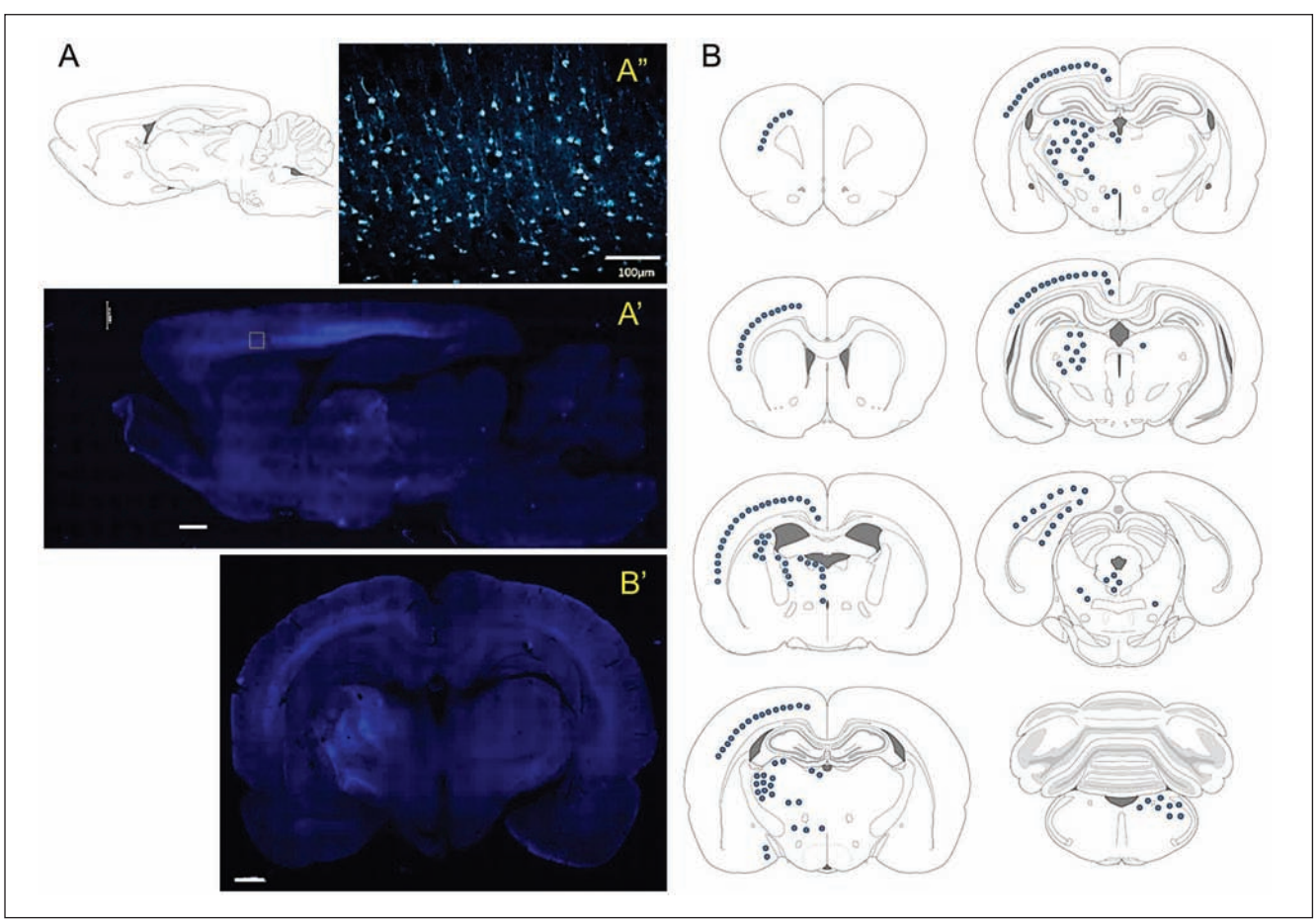

Fig. 5. Fluoro-gold (FG) injected into white matter injury was widely distributed from forebrain to brainstem. (A, A') Scheme of sagittal section 2.40 mm lateral from the midline (A), and FG distribution on the same section (A'). FG was widely distributed in the cortex, thalamus, and brainstem. Neurons labeled with FG in the frontal cortex are shown (A"). (B) Extent of neuronal perikarya mapped with FG on a scheme of coronal sections modified from "The Rat Brain in Stereotaxic Coordinates, 6th ed." (Paxinos and Watson 2007). Blue dots show FG distribution, and detail is shown in Table I. (B') Coronal section 4.3 mm caudal from the bregma showing FG distribution in the cortex and thalamus. Scale bars =1 mm (A', B') and 100 μm (A").

Table I. Distribution of FG-labeled neurons

	Ipsi	Contra
Cerebral cortex		
Motor cortex	+	–
Sensory cortex	+	–
Cingulate cortex	+	–
Granular insular cortex	+	–
Retrosplenial cortex	+	–
Parietal association cortex	+	–
Visual cortex	+	–
Auditory cortex	+	–
Temporal association cortex	+	–
Entorhinal cortex	+	–
Postsubiculum	+	–
Basal ganglia		
Caudate-putamen	+	–
Nucleus accumbens	–	–
Globus pallidus	+	–
Amygdala		
Basolateral nucleus	+	–
Central nucleus	+	–
Medial nucleus	+	–
Thalamus		
Reticular nucleus	+	–
Ventrolateral nucleus	+	–
Ventral anterior nucleus	+	–
Paraventricular nucleus	+	–
Central medial nucleus	+	–
Paratenial nucleus	+	–
Stria medullaris	+	–
Laterodorsal nucleus	+	–
Anterodorsal nucleus	+	–
Anteroventral nucleus	+	–
Lateral posterior nucleus	+	–
Posterior nucleus	+	–
Ventral posterior nucleus	+	–
Central lateral nucleus	+	–
Zone incerta	+	–
Medial habenular nucleus	–	–

	Ipsi	Contra
Hypothalamus		
Supraoptic nucleus	–	–
Suprachiasmatic nucleus	–	–
Ventromedial nucleus	–	–
Posterior nucleus	–	–
Midbrain/brain stem		
Medial pretectal nucleus	+	+
Anterior pretectal nucleus	+	–
Mesencephalic reticular formation	+	–
Substantia nigra	+	–
Dorsal raphe nucleus	+	–
Trochlear nucleus	+	–
Medial longitudinal fasciculus	+	–
Longitudinal fasciculus of the pons	+	–
Superior cerebellar peduncle	–	+
Inferior cerebellar peduncle	–	+
Spinal trigeminal tract	–	+
Facial nucleus	+	+
Vestibular nucleus	–	+
Solitary nucleus	–	+
Hippocampus		
CA1	–	–
CA2	–	–
CA3	–	–
Dentate gyrus	–	–
Olfactory bulb		
Internal granule cell layer	–	–
Mitral cell layer	–	–
Glomerular cell layer	–	–
Cerebellum		
Molecular cell layer	–	–
Purkinje cell	–	–
Granule cell layer	–	–
Additional areas		
Subfornical organ	–	–
Stria terminalis	+	–
Choroid plexus	–	–

Fluoro-Gold (FG) injected into the internal capsule lesion distributed wide area of brain. Ipsi=ipsilateral, contra=contralateral, "+"=distributed, "–"=not distributed.

cause emotional change, but the possibility that WMI may provoke some stress vulnerability leading to depression remains. Although further consideration will be needed in terms of the relationship between WMI and psychiatric disorders, these findings support the idea that this rat lacunar model is likely to have significant similarities with lacunar infarction in patients, even though the motor deficit in the animals is mild and the lesion has wider effects on many systems in the central nervous system not directly manifested as neurological deficits.

Other animal models of white matter injury have been reported in the past. The global hypoperfusion model based on bilateral carotid artery occlusion, and the cerebral small vessel disease model simulating the pathophysiology of the aging brain and induction of white matter injury are such types of models. However, these models also affect the whole brain (including the gray matter), and the lesions mimic more chronic leukoaraiosis rather than sudden onset focal ischemic white matter infarction (Wakita et al. 1994, Kaiser et al. 2014). Selective white matter lesions can be induced by stereotactic injection of ouabain, a Na/K ATPase pump inhibitor, as previously reported (Janowski et al. 2008, Shichinohe et al. 2013, Tan et al. 2015). Ouabain's mechanism of injury is different from that of ischemia, but because the lesion mimics stroke according to MR imaging evaluation, this model may become an equivalent to the ET-1 method of white matter injury (Veldhuis et al. 2003). Recently, new white matter injury models using ET-1 injection have been described, and the correlation between the site of the lesion and motor deficits reported (Blasi et al. 2015). They compared three rat white matter injury models according to the lesion site, from rostral to caudal internal capsule, and only one model with the most caudal lesion showed lasting motor deficits. In our model, the site of ET-1 injection was more rostral compared with that caudal location. Slight differences in the lesion site apparently have different neurological effects in these white matter injury models, which may be important.

The findings of this study that the lesion in the internal capsule affected a much wider neuroanatomical region according to the evaluation with FG was quite unexpected, since the white matter of the rat is known to occupy approximately 10% of the whole brain volume (Frahm et al. 1982), whereas the volume of the lesion was less than 1% of whole brain volume. FG is a fluorescent retrograde axonal tracer, and is taken up by axon terminals or damaged axons, but not by intact undamaged passing fibers (Schmued and Fallon 1986). In spite of this minimal lesion size, the affected axons in the internal capsule showed extensive connections to the ipsilateral hemisphere. Our study found that the neuroanatomical regions associated with axonal damage were located in many cortical areas, including the motor, sensory, and cingulate cortices, thalami, amygdala, and basal ganglia, except for the nucleus accumbens (Table I). Previously, the internal capsule of the rat was reported to connect to the motor/sensory cortex, basal ganglia, and thalamus (Molnár and Cordery 1999). Our study also showed that internal capsule fibers contained projections to the nuclei of the ipsilateral amygdala and midbrain, and to the contralateral cerebellar peduncle and pons. These findings indicate the possibility that white matter lesions have disruptive effects over much wider neuroanatomical regions in terms of effects on the perikarya, although we did not obtain any evidence of the extent of neuronal damage. Therefore, we can assume that the brain with white matter lesions develops potentially multiple system deficits with reduced morphological and functional capabilities that increase its vulnerability under stress compared with the intact brain, although any neurological symptoms and deficits remain subclinical.

The present model induces reproducible white matter damage suitable for studying the pathophysiology of ischemia in the lissencephalic brain and for screening the therapeutic efficacy of drugs, prior to initiating human clinical trials. This model has also an important potential application in cell transplantation experiments for the advancement of stroke therapy. Moreover, this model could be applied to a broader area of the domain of neurosciences, as an experimental cognitive or mood disorder model related to white matter lesions if combined with stress or additional interventions.

CONCLUSIONS

The present modified method of stereotactic injection of ET-1 into the internal capsule of the rat is accurate, reproducible, and safe, and results in a standardized amount of white matter damage in the lissencephalic brain. This study indicates that the experimental model with selective white matter damage has varied applications as a model of subcortical white matter insults associated with multi-system deficits, including conditions not only related to ischemic damage, but also white matter damage associated with cognitive or mood disorders.

ACKNOWLEDGEMENTS

This work was supported by a Grant-in-Aid for Scientific Research (B) to N.S. (No. 25293304), a Grant-in-Aid for Scientific Research (C) to H.I. (No. 25462206), and a Grant-in-Aid for JSPS Fellows to H.O. (No. 13J04334) from the Japan Society for the Promotion of Science. This study is the result of Integrated Research on Neuropsychiatric Disorders carried out under the Strategic Research Program for Brain Sciences by the Ministry of Education, Culture, Sports, Science and Technology of Japan.

REFERENCES

Ben-Shimol E, Gass N, Vollmayr B, Sartorius A, Goelman G (2015) Reduced connectivity and inter-hemispheric symmetry of the sensory system in a rat model of vulnerability to developing depression. Neuroscience 310: 742–750.

Blasi F, Whalen MJ, Ayata C (2015) Lasting pure-motor deficits after focal posterior internal capsule white-matter infarcts in rats. J Cereb Blood Flow Metab 35: 977–984.

Boltze J, Lukomska B, Jolkkonen J, MEMS–IRBI consortium (2014) Mesenchymal stromal cells in stroke: improvement of motor recovery or functional compensation?. J Cereb Blood Flow Metab 34: 1420–1421.

Brown FW, Lewine RJ, Hudgins PA, Risch SC (1992) White matter hyperintensity signals in psychiatric and nonpsychiatric subjects. Am J Psychiatry 149: 620–625.

Chen Y, Imai H, Ito A, Saito N (2013) Novel modified method for injection into the cerebrospinal fluid via the cerebellomedullary cistern in mice. Acta Neurobiol Exp (Wars) 73(2): 304–311.

Debette S, Markus HS (2010) The clinical importance of white matter hyperintensities on brain magnetic resonance imaging: systematic review and meta-analysis. BMJ 341: c3666.

Frahm HD, Stephan H, Stephan M (1982) Comparison of brain structure volumes in Insectivora and Primates. I. Neocortex. J Hirnforsch 23: 375–389.

Frost SB, Barbay S, Mumert ML, Stowe AM, Nudo RJ (2006) An animal model of capsular infarct: endothelin-1 injections in the rat. Behav Brain Res 169: 206–211.

Fuxe K, Kurosawa N, Cintra A, Hallstrom A, Goiny M, Rosen L, Agnati LF, Ungerstedt U (1992) Involvement of local ischemia in endothelin-1 induced lesions of the neostriatum of the anaesthetized rat. Exp Brain Res 88: 131–139.

Gadea A, Schinelli S, Gallo V (2008) Endothelin-1 regulates astrocyte proliferation and reactive gliosis via a JNK/c-Jun signaling pathway. J Neurosci 28: 2394–2408.

Gilmour G, Iversen SD, O'Neill MF, Bannerman DM (2004) The effects of intracortical endothelin-1 injections on skilled forelimb use: implications for modelling recovery of function after stroke. Behav Brain Res 150: 171–183.

Hattori Y, Enmi J, Kitamura A, Yamamoto Y, Saito S, Takahashi Y, Iguchi S, Tsuji M, Yamahara K, Nagatsuka K, Iida H, Ihara M (2015) A novel mouse model of subcortical infarcts with dementia. J Neurosci 35: 3915–3928.

He Z, Yamawaki T, Yang S, Day AL, Simpkins JW, Naritomi H (1999) Experimental model of small deep infarcts involving the hypothalamus in rats: changes in body temperature and postural reflex. Stroke 30: 2743–2751; discussion: 2751.

He Z, Yang SH, Naritomi H, Yamawaki T, Liu Q, King MA, Day AL, Simpkins JW (2000) Definition of the anterior choroidal artery territory in rats using intraluminal occluding technique. J Neurol Sci 182: 16–28.

Imai H, Konno K, Nakamura M, Shimizu T, Kubota C, Seki K, Honda F, Tomizawa S, Tanaka Y, Hata H, Saito N (2006) A new model of focal cerebral ischemia in the miniature pig. J Neurosurg 104: 123–132.

Janowski M, Gornicka-Pawlak E, Kozlowska H, Domanska-Janik K, Gielecki J, Lukomska B (2008) Structural and functional characteristic of a model for deep-seated lacunar infarct in rats. J Neurol Sci 273: 40–48.

Jovicich J, Marizzoni M, Bosch B, Bartres-Faz D, Arnold J, Benninghoff J, Wiltfang J, Roccatagliata L, Picco A, Nobili F, Blin O, Bombois S, Lopes R, Bordet R, Chanoine V, Ranjeva JP, Didic M, Gros-Dagnac H, Payoux P, Zoccatelli G, Alessandrini F, Beltramello A, Bargallo N, Ferretti A, Caulo M, Aiello M, Ragucci M, Soricelli A, Salvadori N, Tarducci R, Floridi P, Tsolaki M, Constantinidis M, Drevelegas A, Rossini PM, Marra C, Otto J, Reiss-Zimmermann M, Hoffmann KT, Galluzzi S, Frisoni GB; PharmaCog Consortium (2014) Multisite longitudinal reliability of tract-based spatial statistics in diffusion tensor imaging of healthy elderly subjects. Neuroimage 101: 390–403.

Kaiser D, Weise G, Moller K, Scheibe J, Posel C, Baasch S, Gawlitza M, Lobsien D, Diederich K, Minnerup J, Kranz A, Boltze J, Wagner DC (2014) Spontaneous white matter damage, cognitive decline and neuroinflammation in middle-aged hypertensive rats: an animal model of early-stage cerebral small vessel disease. Acta Neuropathol Commun 2: 169.

Kim HJ, Im K, Kwon H, Lee JM, Kim C, Kim YJ, Jung NY, Cho H, Ye BS, Noh Y, Kim GH, Ko ED, Kim JS, Choe YS, Lee KH, Kim ST, Lee JH, Ewers M, Weiner MW, Na DL, Seo SW (2015) Clinical effect of white matter network disruption related to amyloid and small vessel disease. Neurology 85: 63–70.

Kissela B, Lindsell CJ, Kleindorfer D, Alwell K, Moomaw CJ, Woo D, Flaherty ML, Air E, Broderick J, Tsevat J (2009) Clinical prediction of functional outcome after ischemic stroke: the surprising importance of periventricular white matter disease and race. Stroke 40: 530–536.

Lecrux C, McCabe C, Weir CJ, Gallagher L, Mullin J, Touzani O, Muir KW, Lees KR, Macrae IM (2008) Effects of magnesium treatment in a model of internal capsule lesion in spontaneously hypertensive rats. Stroke 39: 448–454.

Li X, Liang Y, Chen Y, Zhang J, Wei D, Chen K, Shu N, Reiman EM, Zhang Z (2015) Disrupted frontoparietal network mediates white matter structure dysfunction associated with cognitive decline in hypertension patients. J Neurosci 35: 10015–10024.

Liang H, Yin Y, Lin T, Guan D, Ma B, Li C, Wang Y, Zhang X (2013) Transplantation of bone marrow stromal cells enhances nerve regeneration of the corticospinal tract and improves recovery of neurological functions in a collagenase-induced rat model of intracerebral hemorrhage. Mol Cells 36: 17–24.

Lou M, Yan SQ (2012) The clinical importance and heterogeneity of white matter hyperintensities (in Chinese). Zhonghua Yi Xue Za Zhi 92: 2165–2167.

Maillard P, Carmichael OT, Reed B, Mungas D, DeCarli C (2015) Cooccurrence of vascular risk factors and late-life white-matter integrity changes. Neurobiol Aging 36: 1670–1677.

Maillard P, Fletcher E, Lockhart SN, Roach AE, Reed B, Mungas D, DeCarli C, Carmichael OT (2014) White matter hyperintensities and their penumbra lie along a continuum of injury in the aging brain. Stroke 45: 1721–1726.

Masuda T, Hida H, Kanda Y, Aihara N, Ohta K, Yamada K, Nishino H (2007) Oral administration of metal chelator ameliorates motor dysfunction after a small hemorrhage near the internal capsule in rat. J Neurosci Res 85: 213–222.

Metz GA, Whishaw IQ (2002) Cortical and subcortical lesions impair skilled walking in the ladder rung walking test: a new task to evaluate fore- and hindlimb stepping, placing, and co-ordination. J Neurosci Methods 115: 169–179.

Molnár Z, Cordery P (1999) Connections between cells of the internal capsule, thalamus, and cerebral cortex in embryonic rat. J Comp Neurol 413: 1–25.

Moon SK, Alaverdashvili M, Cross AR, Whishaw IQ (2009) Both compensation and recovery of skilled reaching following small photothrombotic stroke to motor cortex in the rat. Exp Neurol 218: 145–153.

Mortamais M, Artero S, Ritchie K (2013) Cerebral white matter hyperintensities in the prediction of cognitive decline and incident dementia. Int Rev Psychiatry 25: 686–698.

Oshima T, Lee S, Sato A, Oda S, Hirasawa H, Yamashita T (2009) TNF-alpha contributes to axonal sprouting and functional recovery following traumatic brain injury. Brain Res 1290: 102–110.

Paxinos G, Watson C (2007) The Rat Brain in Stereotaxic Coordinates (6th ed.). Academic Press, San Diego, CA, USA.

Petty MA, Wettstein JG (1999) White matter ischaemia. Brain Res Brain Res Rev 31: 58–64.

Porsolt, RD, Le Pichon M, Jalfre M (1977) Depression: a new animal model sensitive to antidepressant treatments. Nature 266: 730–732.

Puentes S, Kurachi M, Shibasaki K, Naruse M, Yoshimoto Y, Mikuni M, Imai H, Ishizaki Y (2012) Brain microvascular endothelial cell transplantation ameliorates ischemic white matter damage. Brain Res 1469: 43–53.

Sasaki Y, Takimoto M, Oda K, Fruh T, Takai M, Okada T, Hori S (1997) Endothelin evokes efflux of glutamate in cultures of rat astrocytes. J Neurochem 68: 2194–2200.

Schallert T, Fleming SM, Leasure JL, Tillerson JL, Bland ST (2000) CNS plasticity and assessment of forelimb sensorimotor outcome in unilateral rat models of stroke, cortical ablation, parkinsonism and spinal cord injury. Neuropharmacology 39: 777–787

Schmued LC, Fallon JH (1986) Fluoro-Gold: a new fluorescent retrograde axonal tracer with numerous unique properties. Brain Res 377: 147–154.

Shichinohe H, Yamauchi T, Saito H, Houkin K, Kuroda S (2013) Bone marrow stromal cell transplantation enhances recovery of motor function after lacunar stroke in rats. Acta Neurobiol Exp (Wars) 73(3): 354–363.

Sozmen EG, Kolekar A, Havton LA, Carmichael ST (2009) A white matter stroke model in the mouse: axonal damage, progenitor responses and MRI correlates. J Neurosci Methods 180: 261–272.

Tan C, Shichinohe H, Abumiya T, Nakayama N, Kazumata K, Hokari M, Hamauchi S, Houkin K (2015) Short-, middle- and long-term safety of superparamagnetic iron oxide-labeled allogeneic bone marrow stromal cell transplantation in rat model of lacunar infarction. Neuropathology 35: 197–208.

Tanaka Y, Akiyoshi J, Kawahara Y, Ishitobi Y, Hatano K, Hoaki N, Mori A, Goto S, Tsuru J, Matsushita H, Hanada H, Kodama K, Isogawa K, Kitamura H, Fujikura Y (2011) Infrared radiation has potential antidepressant and anxiolytic effects in animal model of depression and anxiety. Brain Stimul 4: 71–76.

Tanaka Y, Imai H, Konno K, Miyagishima T, Kubota C, Puentes S, Aoki T, Hata H, Takata K, Yoshimoto Y, Saito N (2008) Experimental model of lacunar infarction in the gyrencephalic brain of the miniature pig: neurological assessment and histological, immunohistochemical, and physiological evaluation of dynamic corticospinal tract deformation. Stroke 39: 205–212.

Ueda Y, Masuda T, Ishida A, Misumi S, Shimizu Y, Jung CG, Hida H (2014) Enhanced electrical responsiveness in the cerebral cortex with oral melatonin administration after a small hemorrhage near the internal capsule in rats. J Neurosci Res 92: 1499–1508.

Ueno M, Hayano Y, Nakagawa H, Yamashita T (2012) Intraspinal rewiring of the corticospinal tract requires target-derived brain-derived neurotrophic factor and compensates lost function after brain injury. Brain 135: 1253–1267.

Veldhuis WB, van der Stelt M, Delmas F, Gillet B, Veldink GA, Vliegenthart JF, Nicolay K, Bar PR (2003) In vivo excitotoxicity induced by ouabain, a Na+/K+-ATPase inhibitor. J Cereb Blood Flow Metab 23: 62–74.

Wagner DC, Scheibe J, Glocke I, Weise G, Deten A, Boltze J, Kranz A (2013) Object-based analysis of astroglial reaction and astrocyte subtype morphology after ischemic brain injury. Acta Neurobiol Exp (Wars) 73(1): 79–87.

Wakita H, Tomimoto H, Akiguchi I, Kimura J (1994) Glial activation and white matter changes in the rat brain induced by chronic cerebral hypoperfusion: an immunohistochemical study. Acta Neuropathol 87: 484–492.

Xu L, Ryu J, Hiel H, Menon A, Aggarwal A, Rha E, Mahairaki V, Cummings BJ, Koliatsos VE (2015) Transplantation of human oligodendrocyte progenitor cells in an animal model of diffuse traumatic axonal injury: survival and differentiation. Stem Cell Res Ther 6: 93.